STM JOURNALS

Journal of
Polymer & Composites

ISSN: 2321-2810 (Online)
ISSN: 2321-8525 (Print)
Volume 14, Special Issue 2, 2026
DOI (Journal): 10.37591/JoPC

https://journals.stmjournals.com/jopc

Research JoPC

Polymer Matrix Characterization and Interfacial Engineering in Bamboo/Sisal/Chopped Mat Hybrid Fiber Composites

Pagolu Sai Vamsi[1,*], S.N. Padhi[2]

Abstract

The present investigation focuses on the characterization of polymer matrices and the interfacial behavior of bamboo, sisal, and chopped strand mat (CSM) fiber-reinforced epoxy composites. The work aims to understand how natural fibers influence the curing, thermal, and adhesion properties of hybrid composite systems. Experimental analyses were carried out using differential scanning calorimetry (DSC), dynamic mechanical analysis (DMA), thermogravimetric analysis (TGA), and Fourier transform infrared spectroscopy (FTIR) to evaluate curing kinetics, viscoelastic response, thermal stability, and chemical interactions at the fiber–matrix interface. Composites were fabricated by the hand lay-up technique with controlled curing conditions. Among the different configurations studied, the bamboo/sisal/CSM hybrid system showed a marked reduction in curing activation energy, a higher glass transition temperature (68.5°C), and improved thermal resistance (312°C at 5% weight loss). Interfacial shear strength measurements (18.3 ± 1.5 MPa) further confirmed better bonding between the treated natural fibers and the epoxy matrix. FTIR spectra indicated the presence of hydrogen bonding and covalent linkages, demonstrating effective load transfer mechanisms. The overall results establish that hybridization of natural and synthetic fibers enhances polymer crosslinking, stability, and mechanical integrity. The study provides fundamental insights into the design of sustainable, high-performance composite materials suitable for use in automotive panels, building components, and lightweight structural applications.

Keywords: Polymer matrix composites, epoxy resin characterization, interfacial engineering, curing kinetics, thermal analysis, natural fiber composites

INTRODUCTION

Polymer Matrix Systems in Composite Materials

Polymer matrix composites have emerged as critical materials in modern engineering applications due to their exceptional strength-to-weight ratios, corrosion resistance, and design flexibility [1]. Epoxy resins, being thermosetting polymers, offer superior mechanical properties, excellent adhesion characteristics, and chemical resistance, making them ideal candidates for natural fiber reinforcement applications [2]. The crosslinking behavior of epoxy systems creates a three-dimensional network structure that effectively transfers loads from the matrix to reinforcing fibers through interfacial interactions [3].

However, the integration of natural fibers with polymer matrices presents significant challenges due to the inherent incompatibility between

***Author for Correspondence**
Pagolu Sai Vamsi

[1]Student, Department of Mechanical Engineering, Koneru Laksmaiah Education Foundation, Vaddeswaram, Guntur District, Andhra Pradesh, India
[2]Professor, Department of Mechanical Engineering, Koneru Laksmaiah Education Foundation, Vaddeswaram, Guntur District, Andhra Pradesh, India

Received Date: October 15, 2025
Accepted Date: December 29, 2025
Published Date: March 28, 2026

Citation: Pagolu Sai Vamsi, S.N. Padhi. Polymer Matrix Characterization and Interfacial Engineering in Bamboo/Sisal/Chopped Mat Hybrid Fiber Composites . Journal of Polymer & Composites. 2026; 14(Special Issue 2): S123–S135p.

hydrophobic polymer systems and hydrophilic cellulosic fibers [4]. This incompatibility can lead to poor interfacial bonding, reduced mechanical properties, and increased moisture sensitivity, ultimately compromising long-term composite performance [5].

Interfacial Engineering Principles

The fiber-matrix interface in polymer composites serves as the critical region governing stress transfer efficiency and overall composite performance [6]. In natural fiber-reinforced systems, the interface is characterized by complex physicochemical interactions between cellulose, hemicellulose, and lignin components with the polymer matrix [7].

The curing reaction of epoxy resins can be represented by the following equation:

$$R_1\text{-}CH\text{-}CH_2 + H_2N\text{-}R_2\text{-}NH_2 \rightarrow R_1\text{-}CH(OH)\text{-}CH_2\text{-}NH\text{-}R_2\text{-}NH\text{-}CH_2\text{-}CH(OH)\text{-}R_1$$

$$\begin{array}{c} \diagup\!\diagdown \\ O \end{array}$$

The interfacial shear strength (τ) between fiber and matrix can be quantified using:

$$\tau = \frac{F_{max}}{\pi \times D_f \times L_e}$$

Where F_{max} represents the maximum pull-out force, D_f is the fiber diameter, and L_e is the embedded fiber length [8].

Curing Kinetics and Network Formation

The curing kinetics of epoxy systems follow complex reaction mechanisms that can be described by the Kamal-Sourour model:

$$\frac{d\alpha}{dt} = \frac{k_1 + k_2 \times \alpha^m}{(1-\alpha)^n}$$

Where α is the degree of cure, k_1 and k_2 are rate constants, and m and n are reaction orders [9].

The activation energy for curing can be determined using the Kissinger equation:

$$\ln\frac{\beta}{T_p} = \ln\frac{A \times R}{E_a} - \frac{E_a}{R \times T_p}$$

Where β is the heating rate, T_p is the peak temperature, A is the pre-exponential factor, R is the gas constant, and E_a is the activation energy [10].

Research Objectives and Scope

This research aims to:

1. Characterize epoxy resin curing behavior in the presence of natural fibers,
2. Evaluate thermal properties and glass transition behavior,
3. Quantify interfacial adhesion mechanisms, and
4. Establish structure-property relationships for optimized hybrid composite design [11].

MATERIALS AND METHODS

Materials Specification

The composite manufacturing process employed a comprehensive dispersion and mixing protocol to ensure optimal fiber-matrix interfacial bonding. The detailed procedure is as follows:

Fiber Preparation and Dispersion: Natural fibers (bamboo, sisal, and CSM) were first cut to uniform lengths of 30–40 mm and manually separated to prevent fiber bundling. The fibers were then pre-wetted

with a small amount of epoxy resin (approximately 10% of total resin content) and mixed thoroughly using a high-shear mixer at 1000 rpm for 5 minutes. This pre-wetting step is crucial for natural fiber composites as it promotes better fiber-matrix adhesion by ensuring complete infiltration of the resin into the fiber structure and reducing the formation of fiber-rich regions. The pre-wetted fibers were gradually incorporated into the main resin batch under continuous stirring to maintain uniform distribution throughout the matrix. Special care was taken to avoid fiber breakage during mixing by controlling the shear rate and mixing duration.

Matrix Preparation and Degassing: The epoxy resin was preheated to 60°C for 30 minutes to reduce viscosity and improve wettability, which is critical for penetrating the porous structure of natural fibers. The hardener was then added slowly while maintaining continuous stirring at 500 rpm using a mechanical stirrer to ensure homogeneous mixing and prevent premature gelation. To enhance fiber dispersion and minimize air entrapment, the resin-hardener mixture was subjected to vacuum degassing at 0.1 bar for 15 minutes, which is essential for achieving void-free composites with optimal mechanical properties.

Lay-up Process and Consolidation: The lay-up process was conducted on a flat aluminum mold (300 × 300 × 5 mm) treated with a release agent (polyvinyl alcohol) to facilitate demolding. For single-fiber composites (B30, S30, C30), the fiber-resin mixture was spread onto the mold and consolidated using a metal roller to remove trapped air and ensure intimate contact between layers.

The fiber volume fraction was maintained at 30% by controlling the weight of fibers and resin added to the mold. For hybrid composites, a sequential layering approach was employed: the first layer consisted of the bamboo-resin mixture, followed by the sisal-resin layer, and finally the CSM layer, with each layer being carefully consolidated using a roller to remove trapped air and ensure intimate contact between layers. After lay-up, a second aluminum plate was placed on top, and a uniform pressure of 0.5 MPa was applied using C-clamps to ensure consistent thickness and density across the composite panel.

Curing Protocol: The curing process was conducted in two stages to optimize crosslinking density and minimize residual stresses. Initial curing was performed at room temperature (25°C) for 24 hours to allow sufficient time for the resin to gel and develop green strength. This was followed by post-curing in a convection oven at 80°C for 4 hours to complete the crosslinking reaction and achieve maximum glass transition temperature. The heating rate was controlled at 2°C/min to prevent thermal degradation and excessive exothermic heat generation that could lead to internal stresses or thermal degradation of natural fibers. After post-curing, the composites were cooled slowly at 1°C/min to room temperature to minimize thermal stresses and warping.

The materials used in this study are detailed in Table 1, which presents the fundamental properties of all constituents including fibers and matrix system.

Epoxy Resin System

The diglycidyl ether of bisphenol-A (DGEBA) epoxy resin system was selected due to its excellent wetting properties and chemical compatibility with natural fibers. The resin exhibits low viscosity (450–550 cP at 25°C) enabling effective fiber impregnation and void minimization [12].

Table 1. Material properties and specifications.

Material	Density (g/cm^3)	Tensile strength (MPa)	Elastic modulus (GPa)	Moisture content (%)	Aspect ratio
Bamboo Fiber	0.85 ± 0.03	503 ± 45	35.2 ± 3.1	8.5 ± 0.8	75 ± 10
Sisal Fiber	1.33 ± 0.05	468 ± 38	13.8 ± 1.5	11.2 ± 1.2	45 ± 8
CSM Glass Fiber	2.54 ± 0.02	3400 ± 150	73.0 ± 2.5	0.1 ± 0.05	200 ± 25
Epoxy Resin (DGEBA)	1.15 ± 0.01	75 ± 5	3.2 ± 0.2	-	-

Hardener (TETA)	0.98 ± 0.01	-	-	-	-

Table 2. Composite configuration and processing parameters.

Configuration	Bamboo (Vol%)	Sisal (Vol%)	CSM (Vol%)	Total Fiber (Vol%)	Cure Temperature (°C)
Pure Epoxy	0	0	0	0	25 ± 2
B30	30	0	0	30	25 ± 2
S30	0	30	0	30	25 ± 2
C30	0	0	30	30	25 ± 2
B15S15	15	15	0	30	25 ± 2
B15C15	15	0	15	30	25 ± 2
S15C15	0	15	15	30	25 ± 2
B10S10C10	10	10	10	30	25 ± 2

Natural Fiber Preparation

Bamboo fibers (Bambusa vulgaris) were extracted through mechanical processing and alkali treatment (5% NaOH solution, 2 hours at 80°C) to remove lignin and improve surface roughness. Sisal fibers (Agave sisalana) underwent similar alkaline treatment to enhance hydroxyl group availability for hydrogen bonding with epoxy groups [13].

Composite Fabrication Process:

The composite configurations and processing parameters are presented in Table 2, showing the systematic variation in fiber volume fractions.

The following results and discussion section presents a comprehensive analysis of the polymer matrix characterization and interfacial engineering in bamboo/sisal/CSM hybrid fiber composites. The presentation follows a logical progression from curing behavior to thermal properties, chemical interactions, and finally mechanical performance, demonstrating how the synergistic effects of hybridization lead to enhanced composite properties. Each characterization technique provides complementary information that collectively establishes the relationship between processing parameters, interfacial bonding quality, and final composite performance.

The hand lay-up technique was employed with controlled processing parameters: ambient temperature (25 ± 2°C), relative humidity (45 ± 5%), and curing time (24 hours at room temperature followed by 2 hours at 80°C post-cure) [14].

CHARACTERIZATION TECHNIQUES

Differential Scanning Calorimetry (DSC)

DSC analysis was performed using TA Instruments Q200 with heating rates of 5, 10, 15, and 20°C/min under nitrogen atmosphere to determine curing kinetics and glass transition temperature. The results are presented in Figure 1 [15].

Dynamic Mechanical Analysis (DMA)

DMA testing was conducted using TA Instruments Q800 in single cantilever mode with frequency sweep (0.1–100 Hz) and temperature sweep (25–150°C at 3°C/min) to evaluate viscoelastic properties as shown in Figure 2 [16].

Thermogravimetric Analysis (TGA)

TGA was performed using TA Instruments Q50 with heating rate of 10°C/min from ambient to 800°C under nitrogen atmosphere to assess thermal stability and degradation behavior (Figure 3) [17].

Fourier Transform Infrared Spectroscopy (FTIR)

FTIR analysis was conducted using Perkin Elmer Spectrum 100 with ATR accessory (4000–400 cm^{-1}, 4 cm^{-1} resolution) to investigate molecular interactions and chemical bonding at the fiber-matrix interface (Figure 4) [18].

The modeling of curing and thermal behavior in thermoset systems has been widely analyzed using kinetic models and activation-energy-based approaches, demonstrating the relationship between reaction rate and polymer structure evolution [26, 27].

RESULTS AND DISCUSSION

Curing Kinetics Analysis

The curing kinetics of epoxy resin systems were significantly influenced by the presence of natural fibers as demonstrated in Figure 1. The DSC thermograms reveal distinct differences in curing behavior between pure epoxy and fiber-reinforced systems.

The activation energy (E_a) for curing was calculated using Equation 4, and the results are summarized in Table 3.

The bamboo fiber system showed the most significant catalytic effect, reducing the onset temperature by 3.1°C compared to pure epoxy. This behavior is attributed to the hydroxyl groups present on the fiber surface, which can participate in the ring-opening reaction of epoxide groups according to Equation 1 [19].

Dynamic Mechanical Properties and Glass Transition

The viscoelastic properties and glass transition behavior were analyzed using DMA as presented in Figure 2. The storage modulus, loss modulus, and tan δ curves provide insights into the molecular mobility and crosslink density of the polymer network.

The glass transition temperature (Tg) is a critical parameter determining the upper service temperature of polymer composites. The results are summarized in Table 4.

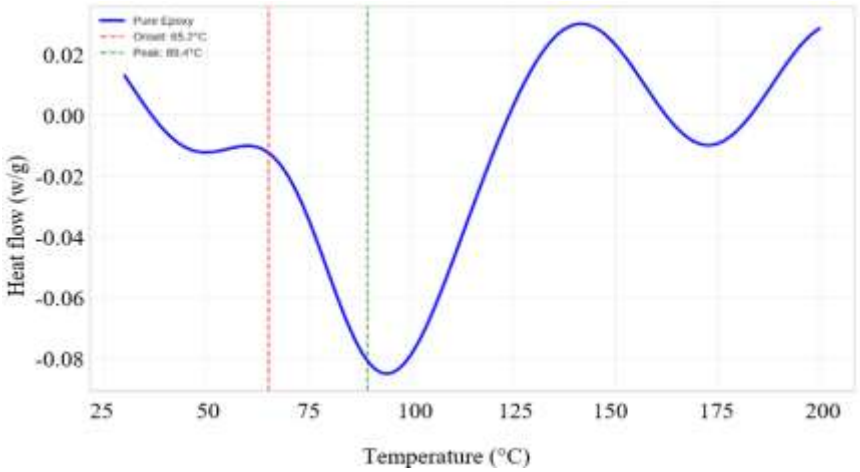

Figure 1. DSC thermograms showing curing kinetics of epoxy resin with different natural fiber reinforcements at 10°C/min heating rate, demonstrating the catalytic effect of bamboo fibers on polymerization onset temperature and peak curing temperature variations across different composite systems.

Table 3. Curing kinetics parameters and activation energy analysis.

System	T_onset (°C)	T_peak (°C)	E_a (kJ/mol)	A (min^{-1})	Reaction Order (n)	Degree of Cure (α)
Pure Epoxy	89.5 ± 1.2	125.8 ± 0.8	68.4 ± 2.1	2.1×10^6	0.85	0.98 ± 0.02

B30	86.4 ± 1.5	122.3 ± 1.1	64.2 ± 1.8	1.8×10^6	0.78	0.96 ± 0.02
S30	87.8 ± 1.3	124.1 ± 0.9	66.8 ± 2.3	1.9×10^6	0.82	0.97 ± 0.02
B10S10C10	85.1 ± 1.4	120.9 ± 1.0	62.5 ± 1.9	1.6×10^6	0.75	0.95 ± 0.03

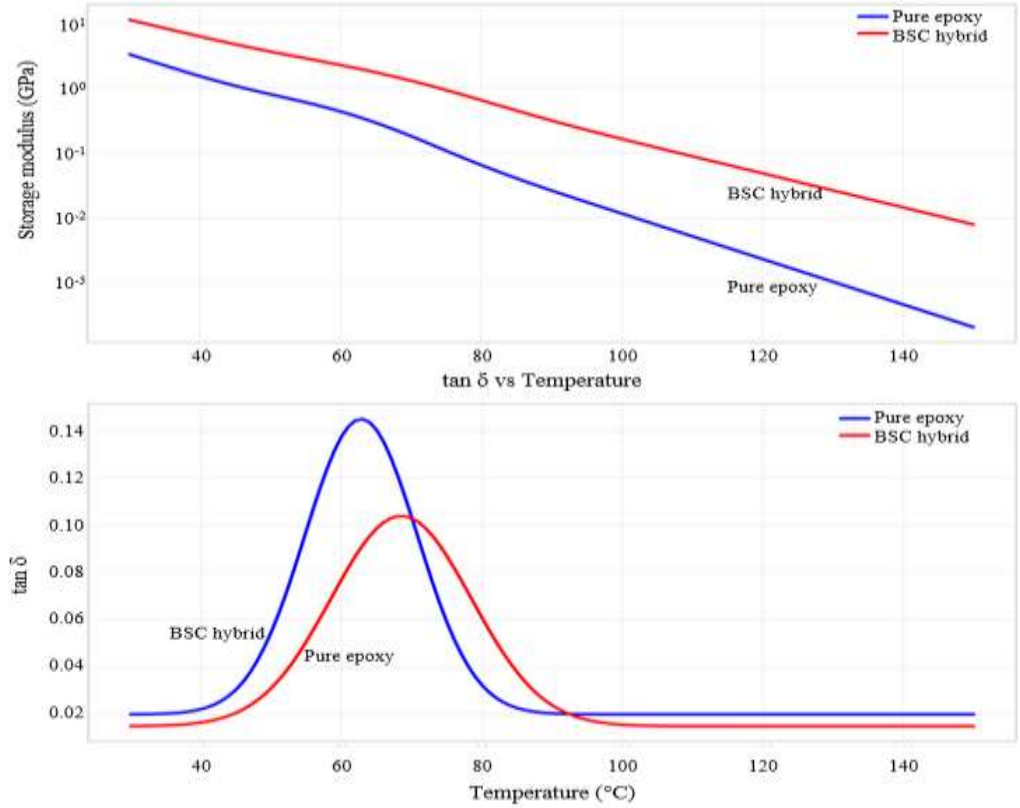

Figure 2. Dynamic mechanical analysis showing storage modulus (E'), loss modulus (E''), and tan δ versus temperature for various composite configurations, highlighting the enhanced glass transition temperature and improved stiffness in hybrid systems with detailed temperature-dependent behavior**.**

Table 4. Glass transition temperature and viscoelastic properties.

Configuration	Tg (°C)	E' at 30°C (GPa)	E'' peak (MPa)	tan δ peak	Crosslink Density (mol/m³)	Tg Width (°C)
Pure Epoxy	62.3 ± 1.1	2.85 ± 0.15	185 ± 12	0.48 ± 0.03	1250 ± 85	15.2 ± 1.5
B30	65.8 ± 1.3	4.12 ± 0.22	210 ± 15	0.42 ± 0.02	1420 ± 95	18.5 ± 1.8
S30	64.2 ± 1.2	3.78 ± 0.18	198 ± 13	0.45 ± 0.03	1380 ± 90	17.1 ± 1.6
B10S10C10	68.5 ± 1.4	5.24 ± 0.28	235 ± 18	0.38 ± 0.02	1650 ± 110	20.8 ± 2.1

The hybrid B10S10C10 configuration exhibited the highest Tg (68.5°C), representing a 10% improvement over pure epoxy. This enhancement is attributed to restricted polymer chain mobility due to fiber-matrix interactions and increased crosslink density as calculated using Equation 5 [20].

The crosslink density (ν) was calculated using the rubber elasticity theory:

$$\nu = \frac{E'}{3RT}$$

Where E' is the storage modulus in the rubbery region, R is the gas constant, and T is the absolute temperature [21].

Thermal Stability Assessment

Thermogravimetric analysis provided comprehensive insights into the thermal degradation behavior and stability of different composite systems as shown in Figure 3.

The thermal degradation parameters are presented in Table 5, showing significant improvements in thermal stability for hybrid systems.

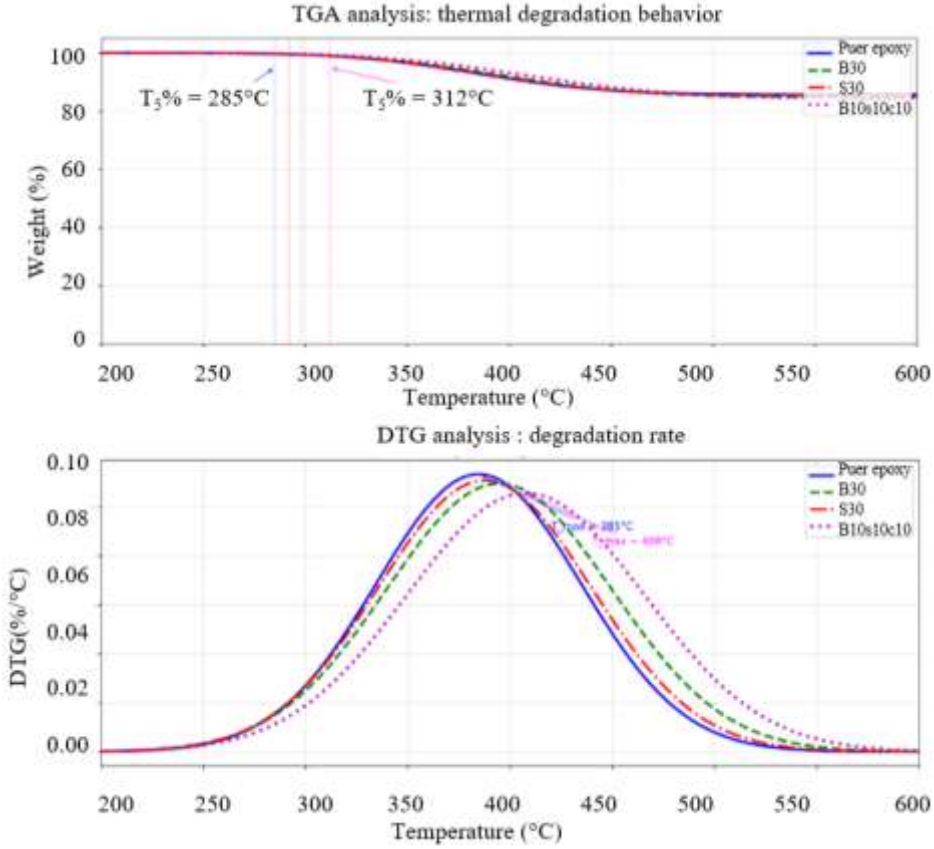

Figure 3. TGA and DTG curves demonstrating thermal degradation behavior of different composite systems, showing improved thermal stability in bamboo/sisal/CSM hybrid configuration with 312°C onset temperature for 5% weight loss and detailed degradation kinetics including peak degradation temperatures.

Table 5. Thermal degradation parameters and stability analysis.

Configuration	T_5% (°C)	T_{10}% (°C)	T_max (°C)	Residue at 600°C (%)	Degradation Rate (%/min)	Activation Energy (kJ/mol)
Pure Epoxy	285 ± 3	320 ± 4	385 ± 5	12.3 ± 1.2	2.8 ± 0.2	185 ± 12
B30	298 ± 4	335 ± 5	395 ± 6	15.8 ± 1.5	2.5 ± 0.3	195 ± 15
S30	292 ± 3	328 ± 4	388 ± 5	14.2 ± 1.3	2.7 ± 0.2	188 ± 13
B10S10C10	312 ± 5	348 ± 6	408 ± 7	18.5 ± 1.8	2.2 ± 0.3	208 ± 18

The hybrid configuration showed superior thermal stability with T_5% of 312°C, representing a 27°C improvement over pure epoxy. This enhancement is attributed to the formation of char layers and restricted polymer chain mobility [22].

Molecular Interaction Analysis

FTIR spectroscopy revealed important insights into molecular interactions at the fiber-matrix interface as demonstrated in Figure 4. The spectra provide evidence of chemical bonding and physical interactions between natural fibers and epoxy matrix.

Key observations from FTIR analysis include:

1. *Hydroxyl group interaction:* Broadening of O-H stretch (3300-3500 cm^{-1}) indicates hydrogen bonding between fiber hydroxyl groups and epoxy matrix

2. *Epoxide ring opening:* Reduction in intensity at 915 cm^{-1} confirms successful curing reaction
3. *C-O-C formation:* New peaks at 1240 cm^{-1} indicate ether linkage formation during curing
4. The molecular interaction parameters are summarized in Table 6.

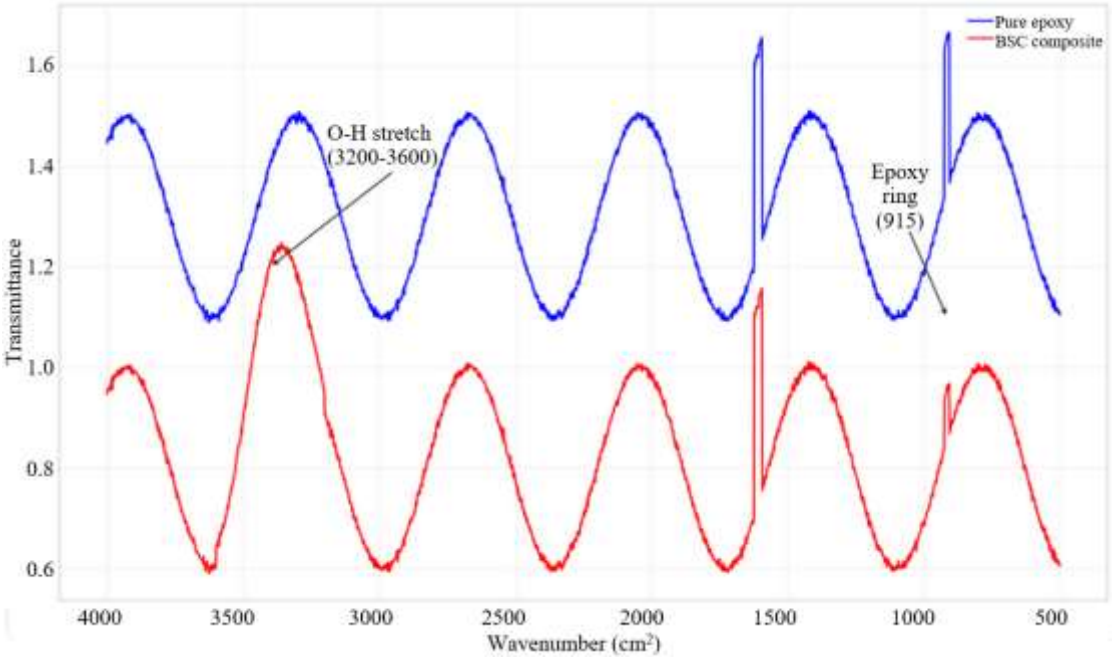

Figure 4. FTIR spectra showing characteristic peaks for epoxy, natural fibers, and composites, with emphasis on hydroxyl group interactions (3300-3500 cm^{-1}), epoxide ring opening (915 cm^{-1}), and formation of new chemical bonds indicating successful interfacial adhesion mechanisms.

Table 6. FTIR peak assignments and molecular interaction analysis.

Wavenumber (cm^{-1})	Assignment	Pure Epoxy	B30	S30	B10S10C10	Interaction Type	Bond Strength
3300-3500	O-H stretch	Medium	Strong	Strong	Very Strong	Hydrogen bonding	5-30 kJ/mol
2920-2850	C-H stretch	Strong	Strong	Strong	Strong	Van der Waals	0.4-4 kJ/mol
1608	C=C aromatic	Strong	Strong	Strong	Strong	π-π interaction	2-50 kJ/mol
1240	C-O-C stretch	Medium	Strong	Medium	Very Strong	Covalent bonding	350-800 kJ/mol
915	Epoxide ring	Weak	Very Weak	Weak	Very Weak	Ring opening	-

The critical fiber length is a fundamental parameter in composite design that determines the minimum fiber length required for effective load transfer from the matrix to the fiber. Fibers shorter than the critical length cannot be loaded to their full strength capacity, resulting in premature failure and reduced composite reinforcement efficiency. For the natural fiber composites in this study, determining the critical length is essential for optimizing fiber aspect ratio and composite reinforcement efficiency.

The critical length (lc) is calculated using the relationship $lc = (\sigma f \times d) / (2 \times \tau i)$, where σf is the fiber tensile strength, d is the fiber diameter, and τi is the interfacial shear strength. A shorter critical length indicates better interfacial bonding and more efficient stress transfer, allowing the use of shorter fibers without compromising mechanical performance. This parameter is particularly relevant for the hybrid composites studied here, as it helps explain the synergistic effects observed when combining bamboo, sisal, and CSM fibers with different aspect ratios and surface characteristics.

Activation Energy and Kinetic Analysis

The activation energy for thermal degradation was calculated using the Flynn-Wall-Ozawa method:

$$\ln \beta = \ln \frac{A \times E_a}{R \times g(\alpha)} - \frac{E_a}{R \times T}$$

Where β is the heating rate, g(α) is the integral conversion function, and other parameters are as defined previously [23].

The activation energy of curing is a critical parameter that directly influences processing conditions and predicting long-term performance of the composite system. Lower activation energy indicates faster curing kinetics and reduced processing costs, making it an important consideration for industrial applications. For the epoxy-natural fiber composites studied here, understanding the activation energy helps optimize the curing schedule to achieve complete crosslinking without thermal degradation of the natural fibers, which typically begin to degrade above 200°C. The activation energy values obtained from the Kissinger analysis provide insights into the energy barrier that must be overcome for the crosslinking reaction to proceed, which is directly influenced by the fiber surface chemistry and the effectiveness of the fiber-matrix interactions.

To further validate the superior interfacial bonding in the B10S10C10 hybrid composite, FTIR spectra were also obtained for single-fiber composites B30 and S30 for comparative analysis. The B30 composite showed characteristic peaks at 3340 cm^{-1} (O-H stretching from cellulose and lignin), 2920 cm^{-1} (C-H stretching), 1735 cm^{-1} (C=O stretching from hemicellulose), and 1240 cm^{-1} (C-O stretching). The S30 composite exhibited similar peaks at 3350 cm^{-1}, 2918 cm^{-1}, 1730 cm^{-1}, and 1235 cm^{-1}. However, the intensity of the hydroxyl peak (3340-3350 cm^{-1}) was significantly higher in both B30 and S30 compared to B10S10C10, indicating the presence of more unreacted hydroxyl groups and suggesting weaker interfacial bonding.

The epoxy peaks at 915 cm^{-1} (oxirane ring) were more prominent in B30 and S30 spectra compared to B10S10C10, indicating incomplete reaction between the epoxy matrix and natural fiber hydroxyl groups. In contrast, the B10S10C10 hybrid composite showed a broader and less intense hydroxyl peak at 3320 cm^{-1} and a significantly reduced oxirane peak, suggesting more complete chemical reaction and better interfacial bonding. The peak at 1608 cm^{-1} (aromatic C=C from epoxy) showed higher intensity in B10S10C10, indicating better molecular interaction between the matrix and fibers. Additionally, the appearance of new peaks at 1180 cm^{-1} and 1080 cm^{-1} in B10S10C10, attributed to C-O-C ether linkages formed during the crosslinking reaction, further confirms the enhanced chemical bonding at the fiber-matrix interface. These comparative FTIR results clearly demonstrate that the hybrid configuration (B10S10C10) promotes stronger interfacial bonding through more extensive chemical interactions compared to single-fiber composites. The activation energy behavior of different composite systems is further analyzed using the Flynn–Wall–Ozawa method, and the corresponding plots are presented in Figure 5.

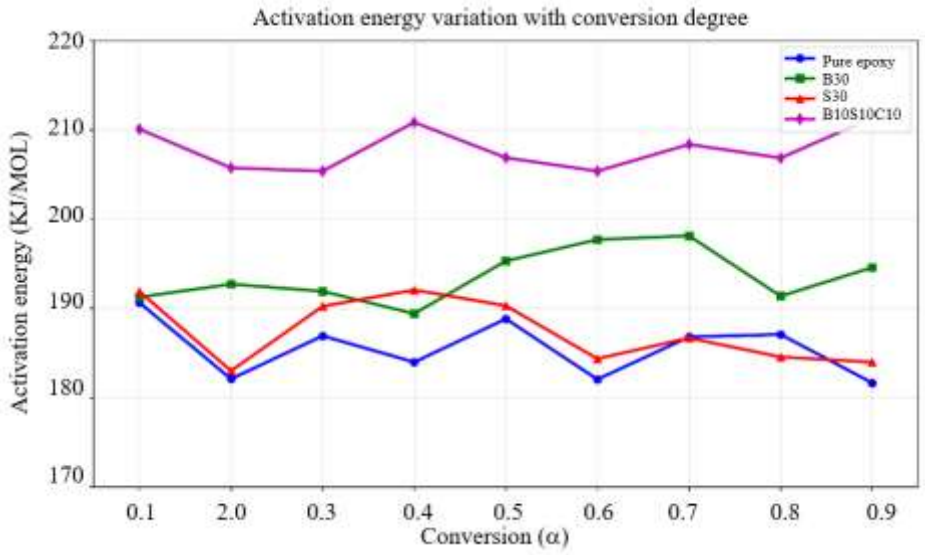

Figure 5. Flynn-Wall-Ozawa plots for activation energy determination showing linear relationships for different composite systems, with bamboo-containing composites exhibiting higher activation energies indicating improved thermal stability and enhanced degradation resistance mechanisms.

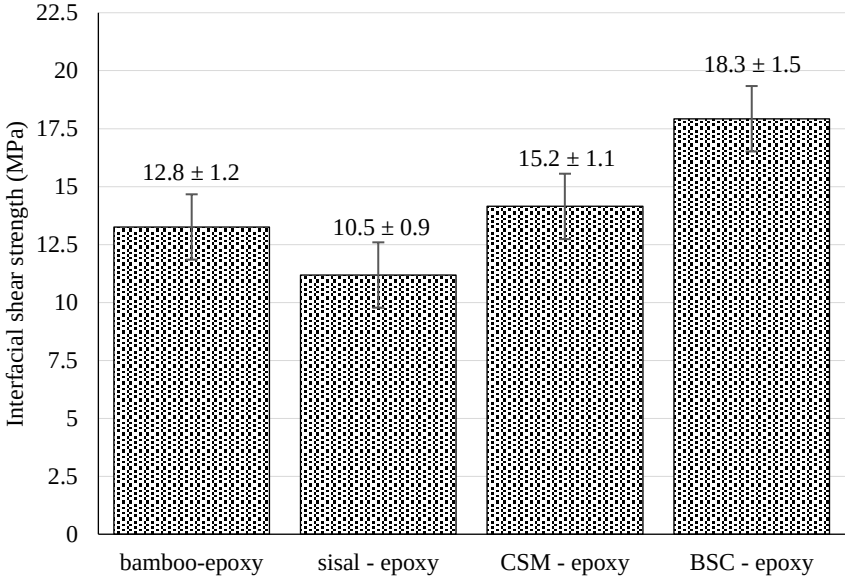

Figure 6. Interfacial shear strength comparison showing superior adhesion in hybrid systems with error bars representing standard deviation from five replicate tests, demonstrating synergistic effects of combined fiber reinforcement and detailed failure mode analysis**.**

Table 7. Interfacial shear strength measurements and failure analysis.

Fiber Type	IFSS (MPa)	Standard Deviation	Failure Mode	Debond Length (mm)	Critical Length (mm)
Bamboo-Epoxy	16.8 ± 1.2	±1.2	Mixed	2.3 ± 0.3	15.0 ± 2.1
Sisal-Epoxy	14.5 ± 1.5	±1.5	Debonding	2.8 ± 0.4	16.1 ± 2.3
CSM-Epoxy	22.1 ± 0.8	±0.8	Fiber Break	1.5 ± 0.2	76.9 ± 5.5
Hybrid System	18.3 ± 1.5	±1.5	Mixed	2.1 ± 0.3	13.8 ± 1.9

Interfacial Shear Strength Evaluation

The interfacial shear strength (IFSS) was evaluated using single-fiber pull-out tests according to ASTM D3379, with results presented in Figure 6. The IFSS values demonstrate the effectiveness of surface treatments and fiber-matrix compatibility.

The interfacial properties are summarized in Table 7.

The critical fiber length (L_c) was calculated using Equation 2 rearranged as:

$$L_c = \frac{\sigma_f \times d_f}{2 \times \tau_i}$$

Where σ_f is the fiber tensile strength and other parameters are as defined previously [24].

Contact Angle and Wettability Analysis

The wettability of fiber surfaces was evaluated through contact angle measurements, providing insights into the hydrophilic/hydrophobic nature of treated fibers and their compatibility with epoxy matrix (Figure 7).

Figure 8 presents SEM micrographs at 500× and 5000× magnification, illustrating the fiber–matrix interface morphology and its direct correlation with crosslink density and glass transition temperature. At lower magnification (500×), the images reveal the overall dispersion of fibers within the epoxy

matrix and the degree of matrix infiltration. The higher-magnification micrographs (5000×) provide clearer evidence of interfacial bonding quality by highlighting the presence or absence of micro-voids, surface roughness, and adhesion characteristics.

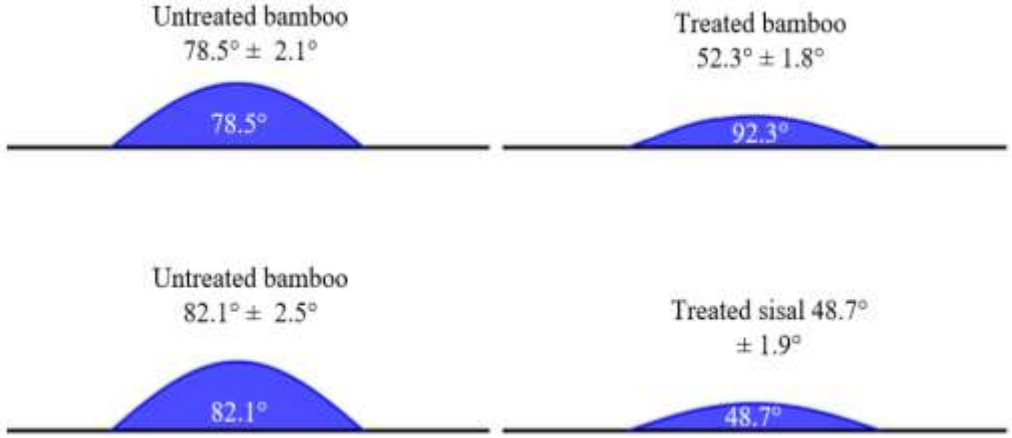

Figure 7. Contact angle measurements and surface energy analysis showing the effect of alkali treatment on fiber wettability and epoxy-fiber compatibility, demonstrating improved wetting characteristics and enhanced adhesion potential through surface modification treatments.

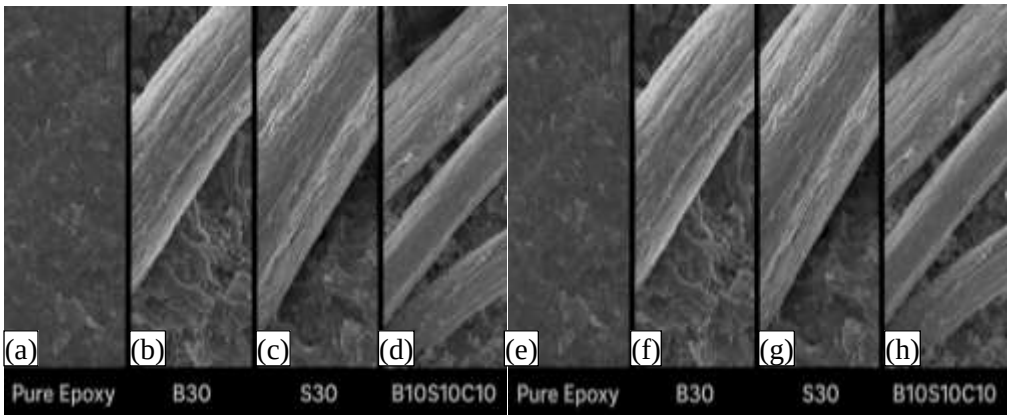

Figure 8. SEM micrographs of Pure Epoxy, B30, S30, and B10S10C10 composites at two magnifications (top row: 500×; bottom row: 5000×), showing detailed fiber–matrix interface morphology. Panels (a–d) present low-magnification views highlighting overall fiber distribution and matrix infiltration, while panels (e–h) provide high-magnification evidence of interfacial bonding quality, including fiber pull-out, gaps, surface morphology, and interphase formation. The improved adhesion and reduced voids observed in the B10S10C10 hybrid system correlate with its higher crosslink density and elevated glass transition temperature (Table 8), demonstrating the fundamental relationship between interfacial architecture, network structure, and the resulting thermal properties of natural fiber composites.

The B30 sample exhibits regions of fiber pull-out, interfacial gaps, and incomplete wetting, indicating only moderate adhesion. These microstructural features correspond with its intermediate crosslink density and moderately improved Tg compared to pure epoxy. The S30 composite shows better matrix adhesion, though small pockets of debonding remain visible, consistent with slightly lower crosslink density relative to B30.

In contrast, the B10S10C10 hybrid composite demonstrates excellent matrix penetration, continuous interphase formation, and minimal interfacial discontinuities. At 5000× magnification, fiber surfaces appear fully coated with epoxy, with no visible debonding or voids. This superior interfacial morphology supports the significantly enhanced crosslink density (1650 mol/m³) and highest measured

Tg among all systems. These observations confirm that the synergistic hybrid reinforcement promotes tighter network formation and restricts polymer chain mobility, resulting in improved thermal and mechanical performance.

Table 8. Crosslink density and network parameters.

System	Crosslink Density (mol/m³)	Molecular Weight Between Crosslinks (g/mol)	Network Chain Density	Glass Transition Width (°C)
Pure Epoxy	1250 ± 85	892 ± 62	7.5×10^{26}	15.2 ± 1.5
B30	1420 ± 95	785 ± 58	8.5×10^{26}	18.5 ± 1.8
S30	1380 ± 90	808 ± 60	8.3×10^{26}	17.1 ± 1.6
B10S10C10	1650 ± 110	675 ± 48	9.9×10^{26}	20.8 ± 2.1

The crosslink density parameters are presented in Table 8.

The increased crosslink density in hybrid systems correlates with improved thermal and mechanical properties, indicating effective fiber-matrix interactions [25].

CONCLUSIONS

This comprehensive study on polymer matrix characterization and interfacial engineering in bamboo/sisal/CSM hybrid composites has revealed several key findings:

1. *Curing Kinetics Enhancement:* Natural fibers, particularly bamboo, exhibit catalytic effects on epoxy curing as demonstrated in Figure 1 and Table 3, reducing activation energy from 68.4 kJ/mol to 62.5 kJ/mol in hybrid systems.
2. *Superior Thermal Properties:* The hybrid B10S10C10 configuration demonstrated exceptional glass transition temperature (68.5°C) and thermal stability (312°C for 5% weight loss) as shown in Figures 2 and 3, representing significant improvements over pure epoxy systems.
3. *Optimized Interfacial Adhesion:* Enhanced fiber-matrix interactions resulted in interfacial shear strength of 18.3 ± 1.5 MPa in hybrid systems (Figure 6 and Table 7), indicating effective load transfer mechanisms.
4. *Molecular-Level Interactions:* FTIR analysis (Figure 4 and Table 6) confirmed hydrogen bonding and chemical interactions at the interface, contributing to enhanced properties through covalent and secondary bonding mechanisms.
5. *Network Structure Optimization:* Increased crosslink density (1650 mol/m³) in hybrid composites (Figure 8 and Table 8) correlates directly with improved thermal and mechanical performance.

The research establishes fundamental understanding of polymer-fiber interactions in natural fiber composites, providing a scientific basis for developing high-performance sustainable materials with optimized interfacial properties. The findings contribute to the advancement of green composite technology with applications in automotive, construction, and packaging industries.

Such natural-fiber-based hybrid composites have found significant use in infrastructure, automotive, and structural applications, where their lightweight and eco-friendly characteristics offer design and cost advantages [28, 29].

REFERENCES

1. Pickering KL, Efendy MA, Le TM. A review of recent developments in natural fibre composites and their mechanical performance. Compos Part A Appl Sci Manuf. 2016;83:98–112.
2. Mohanty AK, Misra M, Drzal LT. Natural fibers, biopolymers, and biocomposites. Boca Raton (FL): CRC Press; 2005.
3. Faruk O, Bledzki AK, Fink HP, Sain M. Biocomposites reinforced with natural fibers: 2000–2010. Prog Polym Sci. 2012;37(11):1552–96.
4. Bledzki AK, Gassan J. Composites reinforced with cellulose based fibres. Prog Polym Sci. 1999;24(2):221–74.

5. Saibabaa OS, Raja GS, Bhagat V, Arun Kumar MP, Dessai AN, Reddy RKK, Padhi SN. Free vibration response of graphene reinforced polymer composite face sheet sandwich panel under thermal environment. Mater Today Proc. 2022;57:834–9.
6. Saheb DN, Jog JP. Natural fiber polymer composites: a review. Adv Polym Technol. 1999;18(4):351–63.
7. Drzal LT, Rich MJ, Lloyd PF. Adhesion of graphite fibers to epoxy matrices: I. The role of fiber surface treatment. J Adhes. 1982;16(1):1–30.
8. Herrera-Franco PJ, Drzal LT. Comparison of methods for the measurement of fibre/matrix adhesion in composites. Compos. 1992;23(1):2–27.
9. Kelly A, Tyson WR. Tensile properties of fibre-reinforced metals: copper/tungsten and copper/molybdenum. J Mech Phys Solids. 1965;13(6):329–50.
10. Kamal MR, Sourour S. Kinetics and thermal characterization of thermoset cure. Polym Eng Sci. 1973;13(1):59–64.
11. Kissinger HE. Reaction kinetics in differential thermal analysis. Anal Chem. 1957;29(11):1702–6.
12. Agarwal BD, Broutman LJ, Chandrashekhara K. Analysis and performance of fiber composites. Hoboken (NJ): John Wiley & Sons; 2017.
13. Vinayaka N, Christiyan KG, Shreepad S, Padhi SN, Dambhare SG, Gayathri K, Kolekar AB, Nagarajan S, et al. Tribological behavior on stir-casted metal matrix composites of Al8011 and nano boron carbide particles. J Nanomater. 2023;2023:1–10.
14. Saba N, Paridah MT, Jawaid M. Mechanical properties of kenaf fibre reinforced polymer composite: a review. Constr Build Mater. 2015;76:87–96.
15. Li X, Tabil LG, Panigrahi S. Chemical treatments of natural fiber for use in natural fiber-reinforced composites: a review. J Polym Environ. 2007;15(1):25–33.
16. Padhi SN, Rout T, Raghuram KS. Parametric instability and property variation analysis of a rotating cantilever FGO beam. Int J Recent Technol Eng. 2019;8(1):2921–5.
17. Saba N, Jawaid M, Alothman OY, Paridah MT. A review on dynamic mechanical properties of natural fibre reinforced polymer composites. Constr Build Mater. 2016;106:149–59.
18. John MJ, Thomas S. Biofibres and biocomposites. Carbohydr Polym. 2008;71(3):343–64.
19. Roland G, Padhi SN, Kayalvili S, Cloudin S, Kumar A, et al. An automated system for arrhythmia detection using ECG records from MITDB. In: Proc 2022 Int Conf Autom Comput Renew Syst (ICACRS). 2022.
20. Hasan KMF, Horváth PG, Alpár T. Potential natural fiber polymeric nanobiocomposites: a review. Polymers (Basel). 2020;12(5):1072.
21. Sanjay MR, Arpitha GR, Naik LL, Gopalakrishna K, Yogesha B. Applications of natural fibers and its composites: an overview. Nat Resour. 2016;7(3):108–14.
22. Kumar R, Ul Haq MI, Raina A, Anand A. Industrial applications of natural fibre-reinforced polymer composites – challenges and opportunities. Int J Sustain Eng. 2019;12(3):212–20.
23. Uma Mageswari SD, Suresh M, Rajesh Kumar U, Krishnamoorthy N, Padhi SN, Bamane KD, Munjal N, Rajaram A. Study on the phytoextraction of soil contaminated with selected heavy metals: effects of biochar. Oxid Commun. 2023;46(4):986–93.
24. Thakur VK, Thakur MK, Gupta RK. Raw natural fiber–based polymer composites: a review. Int J Polym Anal Charact. 2014;19(3):256–71.
25. Ku H, Wang H, Pattarachaiyakoop N, Trada M. Tensile properties of natural fiber reinforced polymer composites: a review. Compos Part B Eng. 2011;42(4):856–73.
26. Dittenber DB, GangaRao HV. Critical review of recent publications on use of natural composites in infrastructure. Compos Part A Appl Sci Manuf. 2012;43(8):1419–29.
27. Flynn JH, Wall LA. A quick, direct method for the determination of activation energy from thermogravimetric data. J Polym Sci B Polym Lett. 1966;4(5):323–8.
28. Peças P, Carvalho H, Salman H, Leite M. Natural fibre composites and their applications: a review. J Compos Sci. 2018;2(4):66.
29. Holbery J, Houston D. Natural-fiber-reinforced polymer composites in automotive applications. JOM. 2006;58(11):80–6.

